Volume 61
Number 83
25 October 2025
Pages 16109–16292

ChemComm

Chemical Communications

rsc.li/chemcomm

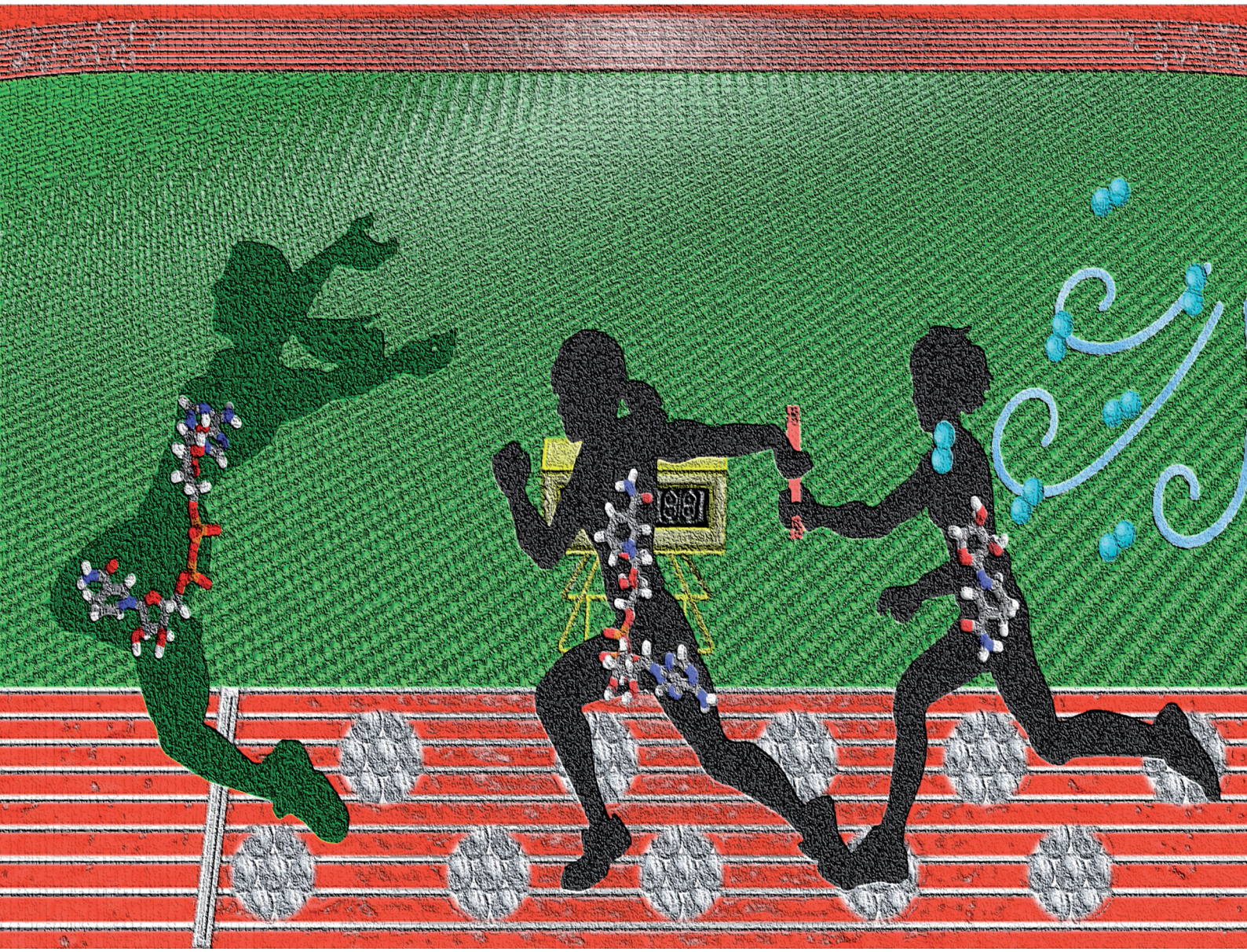

ISSN 1359-7345

ROYAL SOCIETY OF CHEMISTRY

COMMUNICATION

Makoto Hirano, Yutaka Amao *et al.*

Highly selective 1,4-NADH regeneration *via* hydrogenated NAD^+ analogs using a Pt/SiO_2 catalyst with low pressure hydrogen gas

ChemComm

COMMUNICATION

View Article Online
View Journal | View Issue

Cite this: *Chem. Commun.*, 2025, **61**, 16186

Received 26th July 2025,
Accepted 15th September 2025

DOI: 10.1039/d5cc04253d

rsc.li/chemcomm

Highly selective 1,4-NADH regeneration *via* hydrogenated NAD^+ analogs using a Pt/SiO_2 catalyst with low pressure hydrogen gas

Makoto Hirano, *[a] Wataru Onodera,[b] Masazumi Tamura [bc] and Yutaka Amao *[ad]

The hydrogenation of nicotinamide analogs using a Pt/SiO_2 catalyst, followed by hydride transfer to NAD^+, results in the highly selective regeneration of 1,4-NADH. *N*-Methyl nicotinamide exhibits the highest reactivity, achieving 98% selectivity at 20 °C under 1 atm H_2. This strategy provides a practical and sustainable pathway for 1,4-NADH regeneration.

Enzymes catalyze highly selective chemical reactions. Many enzymatic reactions rely on small-molecule cofactors, known as coenzymes, which act as redox mediators within the catalytic cycle.[1] Nicotinamide adenine dinucleotide (NAD^+)—which undergoes hydride addition at the 4-position of its pyridinium ring to form 1,4-dihydronicotinamide adenine dinucleotide (1,4-NADH)—participates in a reversible redox cycle that acts as an essential biological electron carrier in dehydrogenase-catalyzed reactions (Fig. 1a).[2] In industrial enzymatic processes, 1,4-NADH functions as a key reductant but is oxidized back to NAD^+ during the reaction. Efficient NAD^+ regeneration is essential for sustained enzymatic activity. While various methods for NAD^+ regeneration have been explored,[3–17] the hydrogenation method has attracted attention as a green chemistry approach.[6] Furthermore, heterogeneous catalysts offer advantages such as reduced waste generation and easy separation of products from the catalyst,[7] compared with homogeneous catalysts.[8] For example, the Pt/Al_2O_3 catalyst has been used for NAD^+ hydrogenation but has shown limited selectivity (20%)[9] due to undesired byproduct formation, such as the non-biologically active 1,6-dihydro isomer (Fig. S1).[10] The Pt/TiO_2 catalyst improved selectivity (63%),[11] and recent catalysts such as the $Pt\text{-}Sn/SiO_2$ catalyst (90%)[12] and $Rh/Ni\text{–}TiO_2$ catalyst (91%)[13] show further enhancement, though optimization remains (Table S1).

Parallel to the study of NAD^+ hydrogenation, research has focused on understanding the molecular structure of the NAD^+ model[18,19] and designing structural analogs[20–22] or mimic NAD^+s ($mNAD^+$s) (Fig. 1b). These $mNAD^+$s include intermediates found in metabolic pathways, such as nicotinamide mononucleotide (NMN^+).[23,24] Others include synthetic analogs with simplified nicotinamide structures, such as *N*-benzyl nicotinamide (BNA^+)[25] and *N*-methyl nicotinamide (MNA^+).[26] The $mNAD^+$s demonstrate that reduced dihydropyridines donate a hydride specifically to the C4 position of the pyridinium ring, with a *syn* transition state found to be the lowest in energy.[27,28] Notably, 1,4-dihydronicotinamide (1,4-BNAH) has been shown to reduce NAD^+ to 1,4-NADH through C4 hydride delivery and is used as a hydride donor in cofactor recycling.[29,30]

Recently, we reported a Pt/SiO_2-catalyzed hydrogenation system that efficiently converts BNA^+ to 1,4-BNAH with a production rate that is 6.8 times higher than that of 1,4-NADH formation.[31] Based on this, we hypothesized that the hydrogenation of $mNAD^+$ species such as BNA^+ would promote the reduction of NAD^+, enabling the selective formation of 1,4-NADH (Fig. 1c). To evaluate this hypothesis, we investigated the following steps and designed an integrated system: (step 1) hydrogenation of $mNAD^+$ species (NMN^+, BNA^+, MNA^+) using a Pt/SiO_2 catalyst and (step 2) evaluation of the hydride-donating ability of the reduced $mNAD^+$ forms without Pt/SiO_2 catalyst. Finally, one-pot production of 1,4-NADH was performed using the hydrogenated $mNAD^+$s. The system was optimized by adjusting the molar ratio of $mNAD^+$ to NAD^+. Importantly, the entire process proceeds efficiently under low-pressure hydrogen (1 atm), which offers key advantages for integration with enzymatic systems that typically require mild operating conditions.[32] By contrast, the majority of heterogeneous NAD^+ hydrogenation systems reported to date require elevated hydrogen pressures (Table S1). Moreover, operating at ambient pressure enables the direct use of hydrogen generated

[a] *Graduate School of Science, Osaka Metropolitan University, 3-3-138 Sugimoto, Sumiyoshi-ku, Osaka, 558-8585, Japan. E-mail: ss23240i@st.omu.ac.jp, amao@omu.ac.jp*
[b] *Graduate School of Engineering, Osaka Metropolitan University, 3-3-138, Sugimoto, Sumiyoshi-ku, Osaka, 558-8585, Japan*
[c] *Institute of Advanced Energy, Kyoto University, Gokasho, Uji-shi, Kyoto, 611-0011, Japan*
[d] *Research Centre of Artificial Photosynthesis, Osaka Metropolitan University, 3-3-138 Sugimoto, Sumiyoshi-ku, Osaka, 558-8585, Japan*

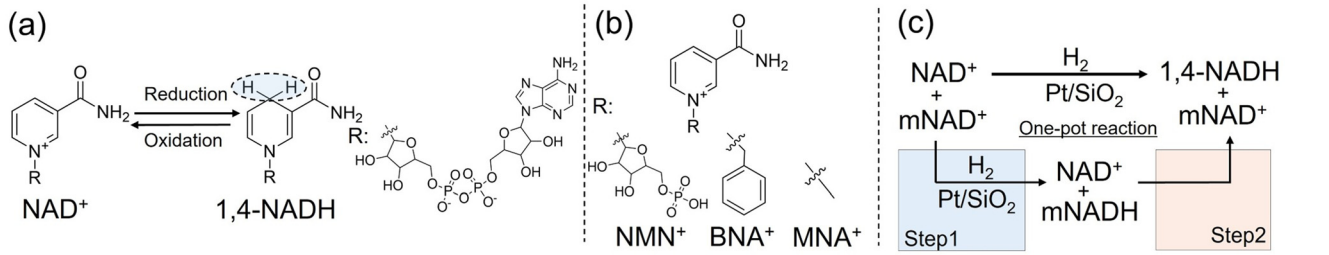

Fig. 1 (a) NAD$^+$ and 1,4-NADH. (b) mNAD$^+$s, including NMN$^+$, BNA$^+$, and MNA$^+$. (c) Schematic of 1,4-NADH production: step 1 involves the Pt/SiO$_2$-catalyzed hydrogenation of mNAD$^+$ to its reduced form (mNADH), followed by step 2, where hydride transfer from mNADH to NAD$^+$ results in the production of 1,4-NADH.

from renewable sources, eliminating compression steps and thereby improving the system's environmental and economic sustainability.[33] This approach thus offers a practical and sustainable strategy for 1,4-NADH regeneration, well-suited for integration into biocatalytic systems.

As a first step, the hydrogenation of mNAD$^+$ species was investigated, as described in step 1 (Fig. 1c). A Pt/SiO$_2$ catalyst with 0.5 wt% was selected based on previous studies.[31] NMN$^+$, BNA$^+$, and MNA$^+$ were employed as mNAD$^+$s based on them being more negative than the NAD$^+$/NADH couple (Table S2). Details of the catalyst preparation and characterization are provided in Fig. S2–S4 and Tables S3–S5, while the full experimental procedures are outlined in Fig. S5–S17 of the SI. Performance parameters were calculated using five equations: conversion (eqn (S1), %), yield (eqn (S2), %), selectivity (eqn (S3), %), production rate of the 1,4-reduced isomers of NAD$^+$ and its analogs (eqn (S4), mmol h^{-1}) and the production rate per Pt surface site (eqn (S5), mmol (mmol Pt_site)$^{-1}$ h^{-1}), hereafter expressed simply as h^{-1}. Based on catalyst characterization, Pt particles were found to have an average size of 2.7–2.8 nm and to be predominantly present as metallic Pt. Hydrogenation was conducted using NAD$^+$, NMN$^+$, BNA$^+$, and MNA$^+$ (each at 1.8 mmol L^{-1}) as substrates in 20 mL of solution containing 10 mg of Pt/SiO$_2$ catalyst under 1 atm H$_2$, 20 °C (Fig. S18–S21). After 130 min, the conversion, yield, and selectivity for the corresponding 1,4-dihydro products (1,4-NADH, 1,4-NMNH, 1,4-BNAH, and 1,4-MNAH) were as follows: NAD$^+$: 33%, 3.1%, and 9.7%; NMN$^+$: 44%, 4.9%, and 11%; BNA$^+$: 65%, 17%, and 25%; MNA$^+$: 77%, 25%, and 32% (Fig. 2). The production rates of the respective 1,4-dihydro species were 12, 11, 94, and 128 h^{-1} for 1,4-NADH, 1,4-NMNH, 1,4-BNAH, and 1,4-MNAH, respectively (Fig. S22). As with 1,4-BNAH, the 1,4-MNAH production rate was higher than that of 1,4-NADH. In contrast, the production rate of NMN$^+$ was comparable to that of NAD$^+$ and significantly lower than those of BNA$^+$ and MNA$^+$. These results suggest that the structural features of the substrates influence their reactivity. In particular, the higher production rate of BNA$^+$ and MNA$^+$ is likely attributable to their simplified molecular structures, which lack the bulky ribose and adenine moieties present in NAD$^+$ and NMN$^+$. The regioselectivity of the hydrogenation products was determined by ^{1}H NMR spectroscopy as hydrogenation can occur at the C4 of the pyridine ring. Hydrogenation reactions of NAD$^+$ and mNAD$^+$s were conducted with

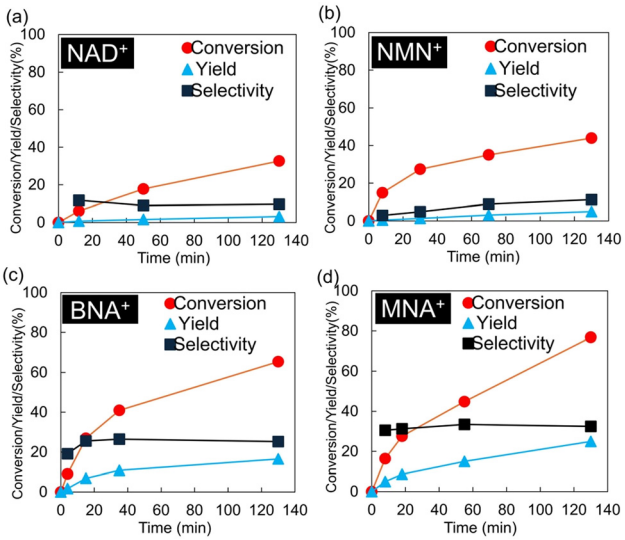

Fig. 2 Hydrogenation of mNAD$^+$s. Reaction conditions: 1.8 mmol L^{-1} (a) NAD$^+$, (b) NMN$^+$, (c) BNA$^+$, or (d) MNA$^+$ in 20 mL of Tris-HCl buffer (pH 8.8), with 20 mg of 0.5 wt% Pt/SiO$_2$ catalyst, under 1 atm H$_2$, 20 °C.

8.0 mmol L^{-1} of NAD$^+$, NMN$^+$, BNA$^+$, or MNA$^+$ in 20 mL of Tris-HCl buffer (pH 8.8) with 20 mg of the Pt/SiO$_2$ catalyst under 1 atm H$_2$, 20 °C. Time-dependent ^{1}H NMR spectra are shown in Fig. S23–S26. NMR and HPLC data showed consistent 1,4-dihydro product concentrations.

To identify suitable mNAD$^+$s for hydride transfer to NAD$^+$, we investigated the reactivity of 1,4-reduced mNAD$^+$ species toward NAD$^+$ and the resulting formation of 1,4-NADH (Fig. 3a). Hydride transfer from 1,4-MNMH, 1,4-BNAH, and 1,4-MNAH (each at 8 mmol L^{-1} in a total reaction volume of 10 mL) to NAD$^+$ (4 mmol L^{-1}) was monitored by ^{1}H NMR spectroscopy (Fig. S27–S29). In all cases, the signals corresponding to the hydride donors and NAD$^+$ gradually decreased over time, while the signal attributed to 1,4-NADH increased accordingly. The time-dependent concentration profiles of 1,4-MNMH, 1,4-BNAH, 1,4-MNAH, and 1,4-NADH are shown in Fig. 3b–d. The initial formation rates of 1,4-NADH (within the first 20 min) were 2.7 × 10^{-3} mmol h^{-1} for 1,4-MNMH, 25 × 10^{-3} mmol h^{-1} for 1,4-BNAH, and 72 × 10^{-3} mmol h^{-1} for 1,4-MNAH (Fig. S30). After 120 min, the yields of 1,4-NADH reached 5.9%, 70%, and

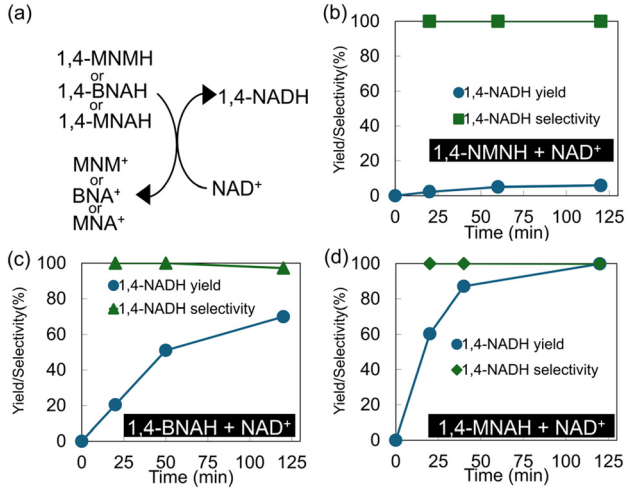

Fig. 3 (a) Production of 1,4-NADH from NAD^+ using 1,4-MNMH, 1,4-BNAH, or 1,4-MNAH as hydride donors. Reaction conditions are 8 mmol L^{-1} of (b) 1,4-MNMH, (c) 1,4-BNAH, or (d) 1,4-MNAH and 4 mmol L^{-1} NAD^+ in 0.1 mol L^{-1} Tris-HCl buffer (pH 8.8) at 20 °C. The reaction volume was 10 mL.

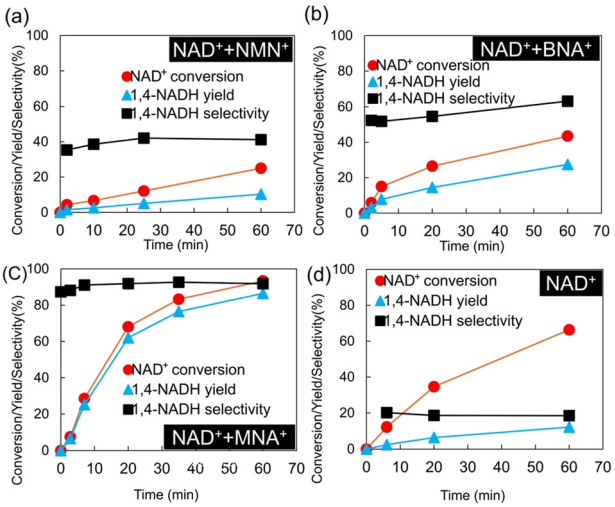

Fig. 4 Production of 1,4-NADH from NAD^+ *via* the hydrogenation of $mNAD^+$s. Reactions were performed with 8 mmol L^{-1} of (a) NMN^+, (b) BNA^+, or (c) MNA^+ and 0.5 mmol L^{-1} NAD^+ in 10 mL of 0.1 mol L^{-1} Tris-HCl buffer (pH 8.8) at 20 °C. (d) 0.5 mmol L^{-1} NAD^+ under the same conditions, without $mNAD^+$.

99% for 1,4-MNMH, 1,4-BNAH, and 1,4-MNAH, respectively, with 1,4-selectivities of 93%, 97%, and 99%, respectively. 1,4-MNAH shows the highest hydride transfer rate, consistent with its redox potential (Table S2).

Next, the effect of the Pt/SiO_2 catalyst on the hydride transfer from hydrogenated MNA^+ to NAD^+, step 2 in the reaction scheme (Fig. 1c), was examined (Fig. S31). A 20-mL solution containing MNA^+ (8 mmol L^{-1}) was hydrogenated over 20 mg of Pt/SiO_2 at 20 °C under 1 atm of H_2 for 30 min. After the reaction, the catalyst was removed by filtration, and the resulting solution was divided into two portions. NAD^+ was added to both solutions to a final concentration of 4 mmol L^{-1}. One of the solutions was then treated with an additional 10 mg of Pt/SiO_2. The 1,4-NADH and 1,4-MNAH concentrations were monitored using ^1H NMR spectroscopy (Fig. S32). The formation rates of 1,4-NADH were 25×10^{-3} mmol h^{-1} in the absence of the catalyst and 28×10^{-3} mmol h^{-1} in its presence, indicating no significant catalytic effect on the hydride transfer from 1,4-MNAH to NAD^+.

Finally, the one-pot conversion of NAD^+ to 1,4-NADH *via* the hydrogenation of $mNAD^+$ (Fig. 1c) was investigated. Reactions were performed in 10 mL of solution containing NAD^+ (0.5 mmol L^{-1}) and either NMN^+, BNA^+, or MNA^+ (each at 8 mmol L^{-1}), using 10 mg of 0.5 wt% Pt/SiO_2 under 1 atm H_2, 20 °C (Fig. 4a–c and Fig. S33–S35). After 60 min, the respective NAD^+ conversion, 1,4-NADH yield, and 1,4-selectivity were as follows: 25%, 10%, and 60% for NMN^+; 43%, 27%, and 63% for BNA^+; and 92%, 87%, and 92% for MNA^+. The production rates were 0.6×10^{-3}, 4.7×10^{-3}, and 7.1×10^{-3} mmol h^{-1} for NMN^+, BNA^+, and MNA^+, corresponding to 5.8, 44, and 68 h^{-1}, respectively (Fig. S36). For comparison, a control experiment using NAD^+ alone under identical conditions showed a conversion of 66%, a 1,4-NADH yield of 12%, and a selectivity of 18% after 60 min (Fig. 4d), with a production rate of 1.2×10^{-3} mmol h^{-1} (12 h^{-1}). These findings clearly demonstrate that the hydrogenation of $mNAD^+$s, particularly MNA^+, over Pt/SiO_2 enables the development of a one-pot system for the efficient and selective conversion of NAD^+ to its enzymatically active form, 1,4-NADH. MNA^+'s high 1,4-NADH productivity likely stems from its superior hydrogenation reactivity and hydride-donating ability. To optimize the concentration of MNA^+, the effect of the MNA^+/NAD^+ molar ratio on the reaction was investigated. The NAD^+ concentration was fixed at 0.5 mmol L^{-1}, while MNA^+ concentrations of 4 and 16 mmol L^{-1} (corresponding to MNA^+/NAD^+ molar ratios of 8 and 32, respectively) were employed. The time-course profiles for each condition are presented in Fig. 5. At an MNA^+ concentration of 4 mmol L^{-1} (molar ratio = 8), the NAD^+ conversion, 1,4-NADH yield, and selectivity after 120 min were 85%, 44%, and 51%, respectively. In contrast, using 16 mmol L^{-1} MNA^+ (molar ratio = 32) yielded values of 88%, 83%, and 96%, respectively, after 60 min. Remarkably, after 3 minutes of reaction, the system reached 16% conversion and 16% yield, with a selectivity of 98%. The corresponding 1,4-NADH production rates for the two concentrations were 1.3×10^{-3} and 14×10^{-3} mmol h^{-1} or

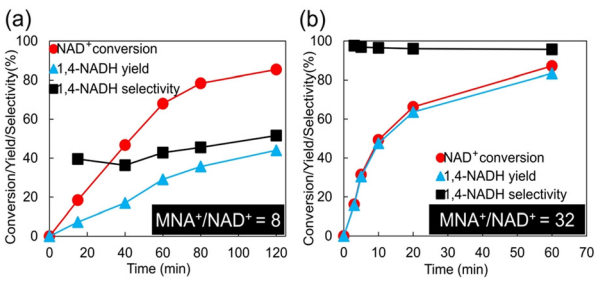

Fig. 5 NAD^+ hydrogenation with different MNA^+/NAD^+ molar ratios. The reaction was carried out in 20 mL of 0.1 mol L^{-1} Tris–HCl Buffer (pH 8.8) containing NAD^+ (0.5 mmol L^{-1}) and MNA^+ at either (a) 4 mmol L^{-1} (MNA^+/NAD^+ = 8) or (b) 16 mmol L^{-1} (MNA^+/NAD^+ = 32), using 10 mg of 0.5 wt% Pt/SiO_2 catalyst under 1 atm H_2 at 20 °C.

12 and 130 h^{-1} (Fig. S37). The concentration of 1,4-MNAH during the reaction was monitored using HPLC (Fig. S38). The 1,4-MNAH concentration profiles (Fig. S39) revealed that higher MNA^+ concentrations led to faster 1,4-MNAH accumulation. These findings indicate that increasing the MNA^+ concentration effectively promotes hydride transfer from 1,4-MNAH to NAD^+.

Comparison of the 1,4-NADH formation rates in Fig. 1c revealed the following trends. In step 1, the hydrogenation of MNA^+ (8 mmol L^{-1}) yielded 1,4-MNAH at a rate of 68 $\times$ 10^{-3} mmol h^{-1}. In step 2, addition of NAD^+ (4 mmol L^{-1}) to the hydrogenated MNA^+ solution yielded a 1,4-NADH formation rate of 28 $\times$ 10^{-3} mmol h^{-1}. In a one-pot system combining steps 1 and 2, a mixture of MNA^+ (8 mmol L^{-1}) and NAD^+ (0.5 mmol L^{-1}) was hydrogenated directly, and the rate was 14 $\times$ 10^{-3} mmol h^{-1}. In contrast, the direct hydrogenation of NAD^+ (0.5 mmol L^{-1}) in the absence of MNA^+ yielded only 9.3 $\times$ 10^{-4} mmol h^{-1} of 1,4-NADH. Although the comparisons are limited by the concentration differences among the setups, these results suggest that MNA^+ is preferentially hydrogenated over NAD^+ on the Pt/SiO_2 catalyst and serves as a selective hydride donor.

We developed a one-pot system for 1,4-NADH regeneration *via* Pt/SiO_2-catalyzed MNA^+ hydrogenation followed by hydride transfer to NAD^+, achieving 98% selectivity and 87% yield at 20 °C and 1 atm H_2 in 60 min. In this study, MNA^+ was used in excess as a hydride shuttle; however, future efforts will focus on improving its hydrogenation selectivity (e.g., through surface modification[34]) to enable $mNAD^+$ to work as a mediator.

This work was partially supported by a Grant-in-Aid for Specially Promoted Research (23H05404), Scientific Research (B) (25K01584), (23K23140), (22H01872), and (22H01871).

Conflicts of interest

There are no conflicts to declare.

Data availability

The data supporting this article have been included as part of the supplementary information (SI). Supplementary information is available. See DOI: **https://doi.org/10.1039/d5cc04253d**.

Notes and references

1 H. Wu, C. Tian, X. Song, C. Liu, D. Yang and Z. Jiang, *Green Chem.*, 2013, **15**, 1773.
2 S. M. A. De Wildeman, T. Sonke, H. E. Schoemaker and O. May, *Acc. Chem. Res.*, 2007, **40**, 1260.
3 P. Wei, Y. Zhang, J. Dong, Y. Cao, S. M. Y. Lee, W. Lou and C. Peng, *Appl. Catal., B*, 2024, **357**, 124257.
4 L. Zhou, Z. Su, J. Wang, Y. Cai, N. Ding, L. Wang, J. Zhang, Y. Liu and J. Lei, *Appl. Catal., B*, 2024, **341**, 123290.
5 S. Fukuzumi, Y. M. Lee and W. Nam, *Chem. Commun.*, 2025, **61**, 3271.
6 X. Wang, T. Saba, H. H. P. Yiu, R. F. Howe, J. A. Anderson and J. Shi, *Chem*, 2017, **2**, 621.
7 T. Saba, J. W. H. Burnett, J. Li, X. Wang, J. A. Anderson, P. N. Kechagiopoulos and X. Wang, *Catal. Today*, 2020, **339**, 281.
8 Y. Maenaka, T. Suenobu and S. Fukuzumi, *J. Am. Chem. Soc.*, 2012, **134**, 367.
9 X. Wang and H. H. P. Yiu, *ACS Catal.*, 2016, **6**, 1880.
10 T. Saba, J. Li, J. W. H. Burnett, R. F. Howe, P. N. Kechagiopoulos and X. Wang, *ACS Catal.*, 2021, **11**, 283.
11 M. Wang, X. Ren, M. Guo, J. Liu, H. Li and Q. Yang, *ACS Sustainable Chem. Eng.*, 2021, **9**, 6499.
12 J. W. H. Burnett, J. Li, A. J. McCue, P. N. Kechagiopoulos, R. F. Howe and X. Wang, *Green Chem.*, 2022, **24**, 1451.
13 M. Wang, H. Dai and Q. Yang, *Angew. Chem., Int. Ed.*, 2023, **62**, e202309929.
14 M. Hall and A. S. Bommarius, *Chem. Rev.*, 2011, **111**, 4088.
15 J. H. Schrittwieser, S. Velikogne, M. Hall and W. Kroutil, *Chem. Rev.*, 2018, **118**, 270.
16 W. Kroutil, H. Mang, K. Edegger and K. Faber, *Curr. Opin. Chem. Biol.*, 2004, **8**, 120.
17 F. Hollmann, I. W. C. E. Arends and K. Buehler, *ChemCatChem*, 2010, **2**, 762.
18 M. A. Viswamitra, *Nature*, 1975, **258**, 540.
19 Y.-D. Wu and K. N. Houk, *J. Org. Chem.*, 1993, **58**, 2043.
20 T. Knaus, C. E. Paul, C. W. Levy, S. de Vries, F. G. Mutti, F. Hollmann and N. S. Scrutton, *J. Am. Chem. Soc.*, 2016, **138**, 1033.
21 C. E. Paul, I. W. C. E. Arends and F. Hollmann, *ACS Catal.*, 2014, **4**, 788.
22 E. King, S. Maxel and H. Li, *Curr. Opin. Biotechnol.*, 2020, **66**, 217.
23 J. Yoshino, J. A. Baur and S. Imai, *Cell Metab.*, 2018, **27**, 513.
24 X. Zhao, N. F. Brown, G. G. López, J. J. Ryan and M. A. J. Finn, *Nat. Chem. Biol.*, 2020, **16**, 87.
25 J. D. Ryan, R. H. Fish and D. S. Clark, *ChemBioChem*, 2008, **9**, 2579.
26 R. J. Knox, F. Friedlos, M. Jarman, L. C. Davies, P. Goddard, G. M. Anlezark, R. G. Melton and R. F. Sherwood, *Biochem. Pharmacol.*, 1995, **49**, 1641.
27 N. Bodor, M. E. Brewster and J. J. Kaminski, *Tetrahedron*, 1988, **44**, 7601.
28 Y.-D. Wu, D. K. W. Lai and K. N. Houk, *J. Am. Chem. Soc.*, 1995, **117**, 4100.
29 K. E. Taylor and J. B. Jones, *J. Am. Chem. Soc.*, 1976, **98**, 5689.
30 L. Josa-Culleré, A. S. K. Lahdenperä, A. Ribaucourt, G. T. Höfler, S. Gargiulo, Y.-Y. Liu, J.-H. Xu, J. Cassidy, F. Paradisi, D. J. Opperman, F. Hollmann and C. E. Paul, *Catalysts*, 2019, **9**, 207.
31 M. Hirano, W. Onodera, M. Tamura and Y. Amao, *Catal. Sci. Technol.*, 2025, **15**, 3806.
32 B. Poznansky, S. E. Cleary, H. A. Reeve and K. A. Vincent, *Front. Chem. Eng.*, 2021, **3**, 718257.
33 G. Lim, D. Calabrese, C. E. Paul and F. Hollmann, *Commun. Chem.*, 2024, **7**, 200.
34 H. Ning, Y. Wu, C. Liu, Z. Zhao, Z. Li, J. Dai, P. Zhang, F. Li, L. Sun and F. Li, *Angew. Chem., Int. Ed.*, 2025, **64**, e202503018.